Applied Catalysis B: Environmental 158–159 (2014) 224–232

Contents lists available at ScienceDirect

Applied Catalysis B: Environmental

journal homepage: www.elsevier.com/locate/apcatb

Effect of photo-corrosion of Ag_2CO_3 on visible light photocatalytic activity of two kinds of Ag_2CO_3/TiO_2 prepared from different precursors

Caixia Feng[a,*], Guoguo Li[a], Pinhong Ren[a], Yan Wang[b], Xianshun Huang[a], Deliang Li[a]

[a] Institute of Environmental and Analytical Sciences, College of Chemistry and Chemical Engineering, Henan University, Kaifeng 475004, PR China
[b] Department of Scientific Research, Henan University, Kaifeng 475001, PR China

ARTICLE INFO

Article history:
Received 5 February 2014
Received in revised form 9 April 2014
Accepted 13 April 2014
Available online 21 April 2014

Keywords:
Ag_2CO_3
Photo-corrosion
Titanium dioxide
Oxygen vacancy
Visible light catalytic activity

ABSTRACT

Two kinds of Ag_2CO_3/TiO_2 nanocomposite photocatalysts, Ag_2CO_3/P25 (P25 refers to TiO_2 of Degussa Company of Germany produced by gas-phase method) and $Ag_2CO_3/TiO_2(V_o^{\bullet})$ ($V_o^{\bullet}$ refers to single-electron-trapped oxygen vacancy (abridged as SETOV)), were prepared by precipitation method with commercial P25-TiO_2 and $TiO_2(V_o^{\bullet})$ as the precursors. The photocatalytic activity of as-prepared Ag_2CO_3/P25 and $Ag_2CO_3/TiO_2(V_o^{\bullet})$ was compared by monitoring the oxidation of propylene under visible light irradiation with pure Ag_2CO_3 photocatalyst as a reference. The oxidation reaction of propylene was performed in two different reaction systems, i.e., a glass reactor combined with a home-made xenon lamp (denoted as system I) and a quartz reactor combined with a commercial xenon lamp (denoted as system II), respectively. Furthermore, X-ray photoelectron spectroscopic analysis, X-ray diffraction analysis, and diffuse reflection spectrometric analysis of Ag_2CO_3/P25 and $Ag_2CO_3/TiO_2(V_o^{\bullet})$ before and after visible light irradiation were conducted to investigate the effect of Ag_2CO_3 photo-corrosion on the activity of the two kinds of photocatalysts, and their photocatalytic mechanisms were proposed. It was found that in system I (light intensity irradiated on to-be-tested samples at $\lambda = 420$ nm: about 9 mW/cm^2), $Ag_2CO_3/TiO_2(V_o^{\bullet})$ shows highly efficient and stable visible light activity and provides a propylene removal rate of up to 90% which remains unchanged within 4 h of irradiation, while the degradation rate of propylene over Ag_2CO_3/P25 is reduced gradually from 35% to nearly zero within 2.5 h of irradiation. In system II (light intensity at $\lambda = 420$ nm: about 40 mW/cm^2), both Ag_2CO_3/P25 and $Ag_2CO_3/TiO_2(V_o^{\bullet})$ exhibit similar photocatalytic activity of up to ca. 90%. Besides, photo-corrosion of Ag_2CO_3 happens during photocatalytic process to afford metallic Ag, and such a photo-corrosion is originally non-conducive to the photocatalysts. Nevertheless, metallic Ag is responsible for strong surface plasmon resonance effect of Ag_2CO_3/P25 and desired electron capture ability of $Ag_2CO_3/TiO_2(V_o^{\bullet})$ as well, leading to highly efficient visible light activity of Ag_2CO_3/P25 in system II. As to $Ag_2CO_3/TiO_2(V_o^{\bullet})$, a large amount of SETOV induces a new sub-band between the valence band and conduction band of $TiO_2(V_o^{\bullet})$, and this sub-band synergistically functions with nascent surface metallic Ag to result in highly visible light activity. Thus the present approach could provide a versatile strategy for the synthesis of novel and efficient visible light-activated photocatalysts.

1. Introduction

Visible-light-driven photocatalysts are of special significance for efficiently utilizing solar energy and indoor light so as to solve energy and environmental dilemmas; and in particular, silver-containing compounds, among numerous photocatalysts, have attracted much attention for their high visible light activity. Kato and coworkers reported that $AgNbO_3$ exhibits photocatalytic activity for O_2 and H_2 evolution from water under visible-light irradiation in the presence of sacrificial reagents [1]. Konta and coworkers prepared silver vanadates (α-$AgVO_3$, β-$AgVO_3$, $Ag_4V_2O_7$ and Ag_3VO_4) by a solid-state and precipitation reaction and found that only Ag_3VO_4 possesses photocatalytic activity for O_2 evolution from an aqueous silver nitrate solution under visible light irradiation [2]. Hu and coworkers claimed that the degradation of target pollutant acid red B in the presence of Ag_3VO_4 synthesized by hydrothermal method confirms the visible light activity of Ag_3VO_4, and the formation of Ag^0 on the surface of the catalyst promotes the

* Corresponding author. Tel.: +86 371 23881589; fax: +86 371 23881589.
E-mail address: caixia8079@henu.edu.cn (C. Feng).

http://dx.doi.org/10.1016/j.apcatb.2014.04.020
0926-3373/

electron–hole separation and interfacial charge transfer thereby leading to increased photocatalytic activity [3]. Usually, researchers attribute the visible light response of the abovementioned Ag-containing complex oxides such as $AgNbO_3$ and Ag_3VO_4 to the decrease in band gap by the valence band (denoted as VB) formation with O 2p and Ag 4d orbital. Recently, Ye and coworkers proposed that Ag- and pentavalent p-block metal (Sb or Bi)-containing complex oxides with strong dispersive effect of VB that consists of less localized s and/or p orbital could be promising visible light sensitive photocatalysts. They found that $AgSbO_3$ with strong dispersive VB exhibits high photocatalytic activity for O_2 evolution and 2-propanol mineralization under visible light irradiation [4]. Maruyama and co-workers compared the photocatalytic properties between α-phase and β-phase $AgGaO_2$ and found that the dispersive VB of the α-phase is advantageous for higher mobility of photogenerated holes thereby imparting stronger oxidization ability [5]. As a new Ag-based photocatalysts, Ag_3PO_4 also exhibits extremely high photooxidative capability for O_2 evolution from water as well as organic dye decomposition under visible light irradiation [6]. Very recently, Ag_2CO_3 semiconductor photocatalyst has been reported to exhibit highly efficient degradation ability for several dyes including Rhodamine B (denoted as RhB), methyl orange and methylene blue [7–9]. However, the abovementioned silver-containing photocatalysts, e.g., Ag_2CO_3, usually undergo photo-corrosion during photocatalysis process, which can seriously deactivate the photocatalysts. Dai and coworkers investigated the photo-corrosion mechanism of Ag_2CO_3 in aqueous solution, and they proposed that silver nitrate, as an excellent electron acceptor, can be used to inhibit the photo-corrosion of Ag_2CO_3 [8]. In this sense, it is imperative to develop novel Ag_2CO_3-based photocatalysts with highly stable visible light photocatalytic activity.

In our recent work, we prepared a $Ag_2CO_3/TiO_2(V_o^{\bullet})$ ($V_o^{\bullet}$ refers to single-electron-trapped oxygen vacancy (abridged as SETOV)) composite photocatalyst with highly stable visible light catalytic activity towards air pollutant decomposition by a facile precipitation route on the surface of anatase $TiO_2(V_o^{\bullet})$ [10]. To reveal the origin of the stable visible light photocatalytic activity of $Ag_2CO_3/TiO_2(V_o^{\bullet})$, in the present research we prepare two kinds of Ag_2CO_3/TiO_2 ($Ag_2CO_3/TiO_2(V_o^{\bullet})$ and Ag_2CO_3/P25 (P25 refers to TiO_2 of Degussa Company of Germany produced by gas-phase method)) and compare their photocatalytic activity by monitoring the oxidation of propylene under visible light irradiation in two different reaction systems. This paper reports the preparation of $Ag_2CO_3/TiO_2(V_o^{\bullet})$ and Ag_2CO_3/P25 as well as the comparison of their visible light catalytic performance for propylene oxidation in relation to Ag_2CO_3 photo-corrosion generating nascent metallic Ag and to formation of SETOV affording a sub-band in $TiO_2(V_o^{\bullet})$ matrix.

2. Experimental

2.1. Catalyst preparation

All chemicals are of analytical grade purity and were used without further purification. Ag_2CO_3 was synthesized at room temperature with the aqueous solutions of $AgNO_3$ and Na_2CO_3 as the starting materials. Briefly, 5 mL of Na_2CO_3 (0.1 M) was added into a 50-mL beaker. Into Na_2CO_3 solution was then slowly added 15 mL of $AgNO_3$ (0.1 M) under 20 min of magnetic stirring to afford yellow precipitate Ag_2CO_3. As-obtained Ag_2CO_3 was filtered, washed with distilled water, and dried at 60 °C in an oven.

$TiO_2(V_o^{\bullet})$ precursor, containing anatase phase TiO_2 and a large amount of SETOV, was prepared by heating nanotubular titanic acid (denoted as NTA) at 600 °C in a tubular furnace for 2 h. The BET specific surface area of $TiO_2(V_o^{\bullet})$ is 87.6 m^2/g, which is slightly larger than that of P25 precursor (54.4 m^2/g). NTA was synthesized according to the method reported elsewhere [11]. Briefly, TiO_2 was allowed to react with concentrated NaOH solution at 120 °C for 24 h under magnetic stirring. When resultant dispersion was naturally cooled down to room temperature, it was washed with de-ionized water and then immersed in 0.1 mol/L HCl solution for 5 h under magnetic stirring. As-obtained product was washed with de-ionized water to remove Cl^-, followed by drying under vacuum at room temperature to afford white powder NTA.

Two kinds of Ag_2CO_3/TiO_2 composites, $Ag_2CO_3/TiO_2(V_o^{\bullet})$ and Ag_2CO_3/P25, were synthesized by the precipitation reaction on the surface of $TiO_2(V_o^{\bullet})$ and P25, respectively. In a typical synthesis, 0.5 g of $TiO_2(V_o^{\bullet})$ (or P25) was dispersed in 10 mL of distilled water and mixed with 5 mL of Na_2CO_3 solution to afford a mixed suspension under ultrasound irradiation. Into resultant mixed suspension was dripped 15 mL of $AgNO_3$ (0.1 M) solution under 20 min of magnetic stirring to yield precipitate. As-obtained precipitate was filtered, washed with distilled water, and dried at 60 °C in an oven to provide desired $Ag_2CO_3/TiO_2(V_o^{\bullet})$ nanocomposite (or Ag_2CO_3/P25).

2.2. Characterization

The morphology of as-prepared photocatalysts was observed with a JEOL JSM-5600LV scanning electron microscope (SEM, accelerating voltage 20 kV) and a JEOL JEM-2010 transmission electron microscope (TEM, accelerating voltage 200 kV). Specific surface areas were determined by using a surface area analyzer (Quadrasorb SI-4). X-ray diffraction (XRD) patterns were measured with a Bruker D8 advance diffractometer. As-prepared catalyst powders and catalyst powder-coated glass plates which were allowed to undergo photocatalytic oxidation test of propylene under visible light irradiation were separately used for XRD analyses (upon the completion of the photocatalytic oxidation test, the amount of the photocatalyst powders scratched from the glass plate is too few to be measured). The ultraviolet–visible light diffusion reflectance spectra (denoted as UV–vis DRS) of the photocatalysts before and after visible light irradiation were recorded with a Shimadzu U-4100 spectrometer and a CARY5000 spectrometer. Electron spin resonance (ESR) spectra were obtained with a Brüker ESP 300E apparatus at a field modulation of 100 kHz, an amplitude modulation of 0.2 mT and a microwave power of 10 mW (the measurement was conducted at room temperature in ambient air, without vacuum-pumping). The g-tensors of the ESR signals were obtained by setting g of diphenyl picryl hydrazyl (DPPH; $g = 2.0036$) as the reference. X-ray photoelectron spectra (XPS) were recorded with a Kratos AXIS Ultra spectrometer using monochromatized Al-$K\alpha$ ($h\nu = 1486.6$ eV) radiation as excitation source. The binding energies were calibrated with reference to adventitious C 1s line at 284.8 eV.

2.3. Evaluation of visible light photocatalytic activity

The visible light photocatalytic activity of Ag_2CO_3, Ag_2CO_3/P25 and $Ag_2CO_3/TiO_2(V_o^{\bullet})$ samples was evaluated by monitoring the oxidation of propylene in reaction system I and reaction system II, respectively. Reaction system I involves a glass reactor combined with a home-made xenon lamp (intensity is 9 mW/cm^2 at $\lambda = 420$ nm) as the visible light source, while reaction system II contains a quartz reactor combined with a commercial xenon lamp (intensity is 40 mW/cm^2 at $\lambda = 420$ nm). The structure of the glass reactor in system I is the same with that of quartz reactor in system II, as shown in Fig. S1. In both reaction systems, 25 mg aliquot of each to-be-tested photocalyst samples was spread on one side of a roughened glass plate (about 8 cm^2) located in the reactor. Between the xenon lamp and reactor was inserted an UV-cut 420 filter to eliminate UV. Both reactors were surrounded by a water channel so as to eliminate infrared light and keep a constant

reaction temperature. The flow rate of the feed gas (pure C_3H_6 and dry air stored in high-pressure cylinders; C_3H_6 concentration: about 500 ppmV) is 200 mL/h. The volume of two reactors (glass and quartz reactor with a same length of 12 cm) affording the feed gas to pass through is 14 and 55 mL, respectively. When the flow rate of the feed gas was chosen as 200 mL/h, the residence time of gas flowing through two reactors is ca. 4 and 16 min accordingly. Considering light irradiation on to-be-test sample is only about half length of two reactors (6 cm), the actual contact time between feed gas and catalyst under irradiation in two reactors is ca. 2 and 8 min, respectively. Prior to irradiation, the feed gas was allowed to flow through the reactor continuously until the adsorption/desorption equilibrium was established. The on-line concentration of C_3H_6, C, was determined by a chromatograph (GC7900) equipped with a flame ionization detector (FID), a GDX-502 column, and a reactor loaded with Ni catalyst for the methanization of CO_2. The removal rate of C_3H_6 is calculated as $(C_0 - C)/C_0 \times 100\%$, where C_0 refers to the initial C_3H_6 concentration (500 ppmV).

3. Results and discussions

3.1. Characteristics of various as-prepared photocatalysts

SEM photograph of as-prepared Ag_2CO_3 is shown in Fig. 1a. It can be seen that as-prepared Ag_2CO_3 consists of short rods with a length of about 1 μm and a diameter of 400 nm as well as a small amount of irregular particles, which is in well agreement with what is reported elsewhere [7]. Fig. 1b and c shows typical TEM images of as-prepared $Ag_2CO_3/TiO_2(V_o^{\bullet})$ and Ag_2CO_3/P25, respectively. It can be seen that as-prepared $Ag_2CO_3/TiO_2(V_o^{\bullet})$ consists of $TiO_2(V_o^{\bullet})$ nanorods with a diameter of about 10 nm (they are generated by 2 h heat-treatment at 600 °C of NTA whose tubular structure is broken thereat) and superfine Ag_2CO_3 nanoparticles (average size 2–3 nm) evenly dispersed on the surface (Fig. 1b). Similar to $Ag_2CO_3/TiO_2(V_o^{\bullet})$, as-prepared Ag_2CO_3/P25 also contains uniformly-dispersed Ag_2CO_3 nanoparticles with an average diameter of 3–4 nm on the surface (Fig. 1c). It can be supposed that such fine Ag_2CO_3 nanoparticles on the surface of $Ag_2CO_3/TiO_2(V_o^{\bullet})$ and Ag_2CO_3/P25 might exhibit much better photocatalytic performance than micro-sized Ag_2CO_3.

Fig. 2a shows the XRD patterns of NTA and $TiO_2(V_o^{\bullet})$. It can be seen that all the XRD peaks of NTA can be assigned to (2 0 0), (1 1 0) and (0 2 0) planes of orthorhombic phase, as it is elucidated elsewhere [11–14]. After NTA is annealed at 600 °C for 2 h, anatase phase $TiO_2(V_o^{\bullet})$ is obtained, which indicates that orthorhombic phase of NTA is easily destroyed and transformed into anatase TiO_2 during annealing at 600 °C. Fig. 2b shows the XRD patterns of Ag_2CO_3, $Ag_2CO_3/TiO_2(V_o^{\bullet})$ and Ag_2CO_3/P25. All the diffraction peaks of Ag_2CO_3 can be indexed to those of monoclinic phase structure, which well conforms to that reported elsewhere [7]. Both as-prepared Ag_2CO_3/P25 and $Ag_2CO_3/TiO_2(V_o^{\bullet})$ show the diffraction peaks of TiO_2 (Ag_2CO_3/P25 contains both anatase and rutile phases, and $Ag_2CO_3/TiO_2(V_o^{\bullet})$ contains only anatase phase) and those characteristic diffraction peaks of monoclinic Ag_2CO_3, which indicates that Ag_2CO_3 particles have been deposited on the surface of P25-TiO_2 and $TiO_2(V_o^{\bullet})$ matrix.

Fig. 3 displays the ESR spectra of Ag_2CO_3, $Ag_2CO_3/TiO_2(V_o^{\bullet})$ and Ag_2CO_3/P25. No ESR signals are observed for Ag_2CO_3 and Ag_2CO_3/P25, which indicates that they are free of paramagnetic species. Differing from Ag_2CO_3 and Ag_2CO_3/P25, $Ag_2CO_3/TiO_2(V_o^{\bullet})$ prepared with $TiO_2(V_o^{\bullet})$ as the precursor exhibits ESR signal with $g = 2.004$ owing to the formation of SETOV during the annealing process of NTA [12–17], which indicates that as-prepared $Ag_2CO_3/TiO_2(V_o^{\bullet})$ contains intrinsic solid defect (i.e., SETOV) that is

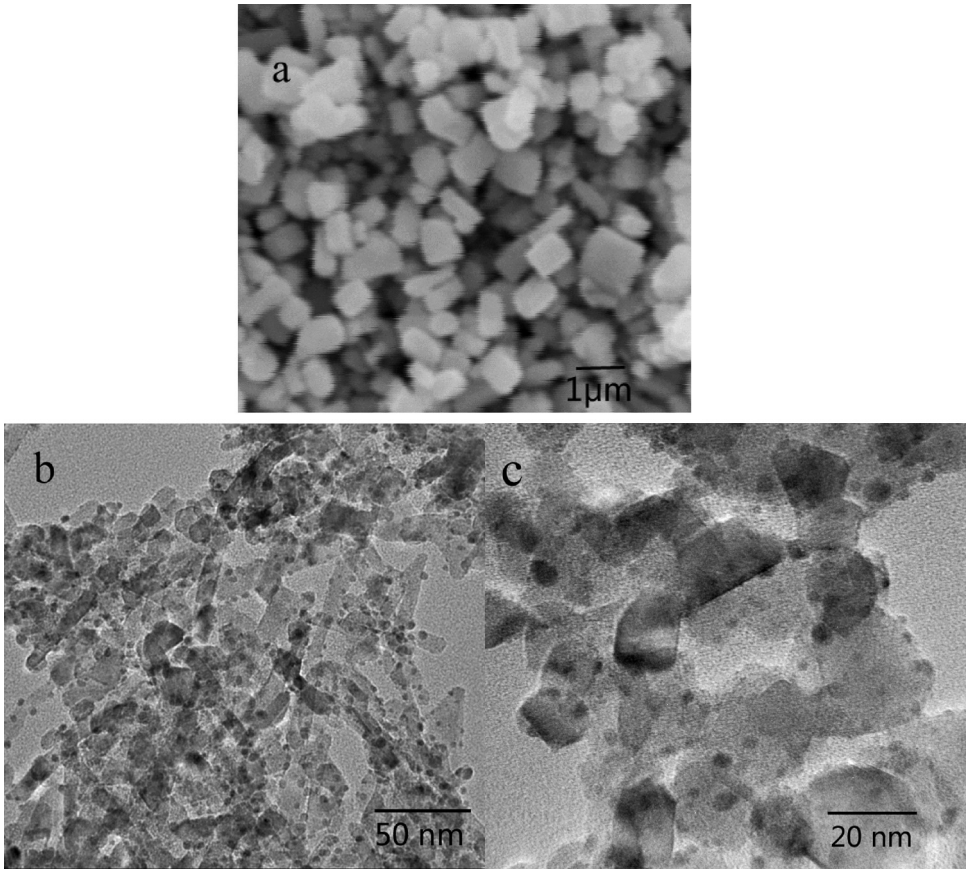

Fig. 1. SEM image (a) of sample Ag_2CO_3 as well as typical TEM images of $Ag_2CO_3/TiO_2(V_o^{\bullet})$ (b) and Ag_2CO_3/P25 (c).

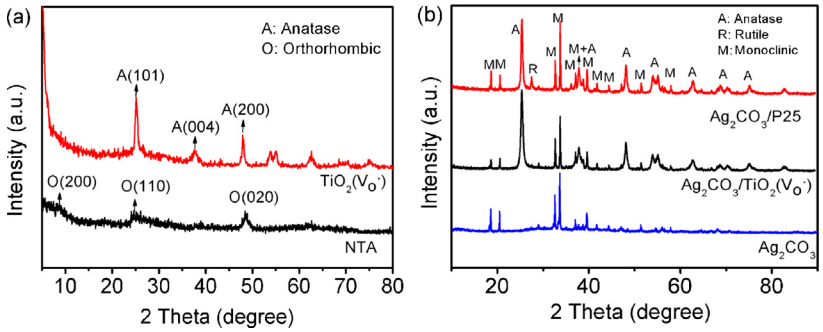

Fig. 2. XRD patterns of (a) NTA and $TiO_2(V_o^{\bullet})$ and (b) Ag_2CO_3, $Ag_2CO_3/TiO_2(V_o^{\bullet})$ and Ag_2CO_3/P25.

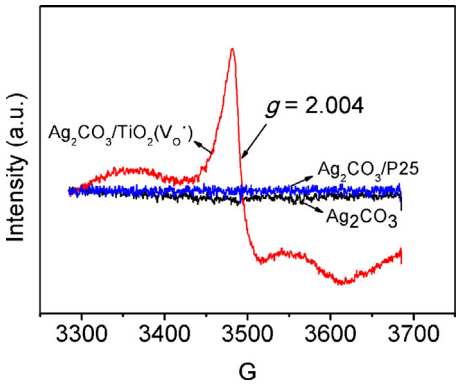

Fig. 3. ESR spectra of Ag_2CO_3, $Ag_2CO_3/TiO_2(V_o^{\bullet})$ and Ag_2CO_3/P25 (the results are obtained at room temperature in air atmosphere).

absent in Ag_2CO_3 and Ag_2CO_3/P25. A large amount of SETOVs generated in $Ag_2CO_3/TiO_2(V_o^{\bullet})$ may result in a new sub-band below the conduction band of $TiO_2(V_o^{\bullet})$ matrix. Upon visible light excitation, the electrons trapped by SETOV can be excited to the conduction band and compensated with the valence band electron thereby leaving holes in the valence band. As a result, the electron–hole pair can be generated for the new sub-band resulted from SETOV under visible light irradiation.

The UV–vis DRS of as-prepared Ag_2CO_3, Ag_2CO_3/P25 and $Ag_2CO_3/TiO_2(V_o^{\bullet})$ are shown in Fig. 4, where the absorption spectrum of commercial P25-TiO_2 is also given for a comparison. P25-TiO_2 has no any absorption in visible light region, which is consistent with what is displayed in Fig. 4. As-prepared Ag_2CO_3 shows an absorption edge around 480 nm, which suggests that it can be excited by visible light. As-prepared Ag_2CO_3/P25 shows apparent visible light absorption, due to the deposition of Ag_2CO_3 nanoparticles on the surface of P25-TiO_2. Moreover, as-prepared photocatalyst $Ag_2CO_3/TiO_2(V_o^{\bullet})$ shows strong visible light absorption especially in the range of 400–500 nm, which implies that there might exist synergistic photocatalytic effect between surface deposited Ag_2CO_3 and oxygen vacancies in $TiO_2(V_o^{\bullet})$ matrix.

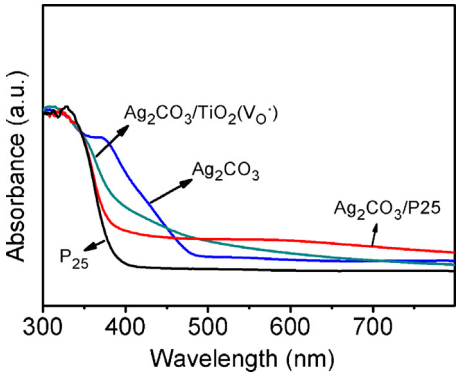

Fig. 4. UV–vis absorption spectra of samples P25, Ag_2CO_3, $Ag_2CO_3/TiO_2(V_o^{\bullet})$ and Ag_2CO_3/P25.

3.2. *Visible light photocatalytic activity and photo-corrosion in reaction systems I and II*

Recently, with the fantastic spur both in industry and in economy in China, more and more cars are produced and run in the street. A large volume of poisonous gas, especially uncompleted combustion hydrocarbons will be given off. Propylene, the typical hydrocarbon, was chosen as target to be decomposed by photocatalyst in this paper. Fig. 5a shows the visible light photocatalytic activity of samples Ag_2CO_3, Ag_2CO_3/P25 and $Ag_2CO_3/TiO_2(V_o^{\bullet})$ towards degradation of propylene in system I. On the one hand, as the xenon lamp is turned on under the catalysis by Ag_2CO_3 and Ag_2CO_3/P25, high removal rates of propylene (70% and 35%) are obtained. However, with the increase of irradiation time, the

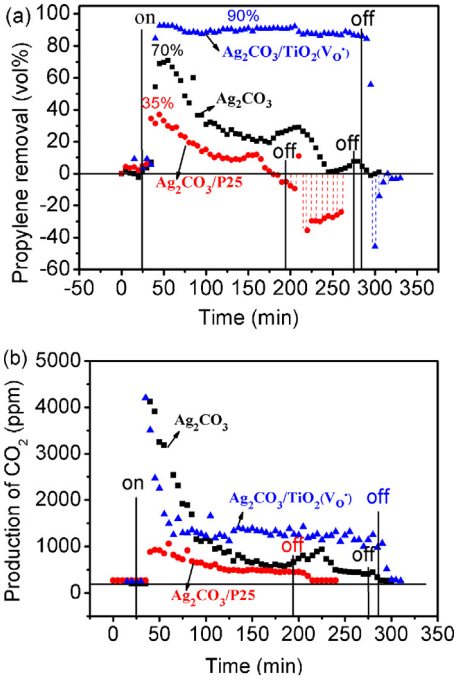

Fig. 5. Degradation of propylene (a) in association with production of CO_2 (b) over samples Ag_2CO_3, $Ag_2CO_3/TiO_2(V_o^{\bullet})$ and Ag_2CO_3/P25 in system I. (a home-made xenon lamp is used as light source, and the glass reactor is surrounded by a cooling-water channel to eliminate infrared light. A cut filter with $\lambda \geq 420$ nm is inserted between the xenon lamp and the glass reactor to eliminate UV light. The light intensity of $\lambda = 420$ nm irradiated on sample is ca. 9 mW/cm^2).

removal rates of propylene over both photocatalysts gradually decline to nearly zero. Furthermore, as the xenon lamp is turned off, the removal rate of propylene over Ag_2CO_3/P25 is lowered down to −35.6%. This illustrates that, just as the xenon lamp is turned on, a part of propylene (up to 35%) is instantly photo-adsorbed on the surface of Ag_2CO_3/P25, and then it is desorbed from the photocatalyst surface upon turning off of the xenon lamp. Such a photo-induced adsorption–desorption of propylene has been observed over Ag/TiO_2 nanotube [18]. On the other hand, after the xenon lamp is turned on, the degradation rate of propylene over Ag_2CO_3/TiO_2(V_o•) remains above 90% within 4 h of visible light irradiation. Naturally, as the xenon lamp is turned off, propylene on the surface of Ag_2CO_3/TiO_2(V_o•) undergoes similar desorption behavior that is observed over Ag_2CO_3/P25. However, the desorption amount from Ag_2CO_3/TiO_2(V_o•) estimated from the integrated area (252; marked by blue dash line in Fig. 5a) is much less than that from Ag_2CO_3/P25 (2170; marked by red dash line in Fig. 5a). This demonstrates that, as the light is turned off, much less propylene is desorbed from the surface of photocatalyst Ag_2CO_3/TiO_2(V_o•) rather than Ag_2CO_3/P25. As a result, Ag_2CO_3/TiO_2(V_o•) exhibits more stable and better photocatalytic activity than Ag_2CO_3/P25 towards degradation of propylene under visible light irradiation. The BET specific surface areas of both TiO_2 precursors, TiO_2(V_o•) and P25, are 87.6 and 54.4 m^2/g, respectively. After depositing Ag_2CO_3 by precipitation method, big change would not happen from precursor TiO_2 to Ag_2CO_3/TiO_2. So, The specific surface area of Ag_2CO_3/TiO_2(V_o•) should be slightly larger than that of Ag_2CO_3/P25. Considering the BET areas, the photocatalytic activity of Ag_2CO_3/TiO_2(V_o•) is still much higher than that of Ag_2CO_3/P25. To explore the deactivation reasons of Ag_2CO_3 and Ag_2CO_3/P25 and further confirm the stable photocatalytic activity of Ag_2CO_3/TiO_2(V_o•), we monitored the change of CO_2 concentration generated during the photocatalytic process and plotted it as a function of irradiation time. As shown in Fig. 5b, the concentration of produced CO_2 over both Ag_2CO_3 and Ag_2CO_3/P25 declines gradually with the increase of irradiation time and tends to be close to the initial level before irradiation, which is consistent with the change of propylene removal rate shown in Fig. 5a. What is worth special emphasis is that, although the concentration of produced CO_2 over Ag_2CO_3/TiO_2(V_o•) also declines after the xenon lamp is turned on, it retains a steady value of about 1300 ppm after 50 min of visible light irradiation. Noticing that the complete oxidation of 1 mol of C_3H_6 should generate 3 mol of CO_2, we can infer that photo-degraded propylene (500 ppm × 90%) is completely mineralized to yield CO_2. Namely, CO_2 selectivity over Ag_2CO_3/TiO_2(V_o•) is even as much as 100%.

In order to further test the photocatalytic activity and stability of samples Ag_2CO_3, Ag_2CO_3/P25 and Ag_2CO_3/TiO_2(V_o•), we conducted recycle experiments of propylene degradation over these photocatalysts in system II (light intensity of λ = 420 nm is 40 mW/cm^2). As shown in Fig. 6, both the degradation rate of propylene (Fig. 6a) and the production of CO_2 (Fig. 6b) over Ag_2CO_3 decrease gradually with the increase of irradiation time in cycle 1, which is similar to that observed in reaction system I. In the next three cycles, the propylene removal rate over Ag_2CO_3 is reduced to only about 10%, due to the photo-corrosion of Ag_2CO_3 under visible light irradiation. Ag_2CO_3/P25 exhibits high and stable photocatalytic activity under visible light irradiation (Fig. 6c and d), and the propylene removal rate reaches 93% in cycle 1, which is very different from that observed in reaction system I. In the next four cycles, the

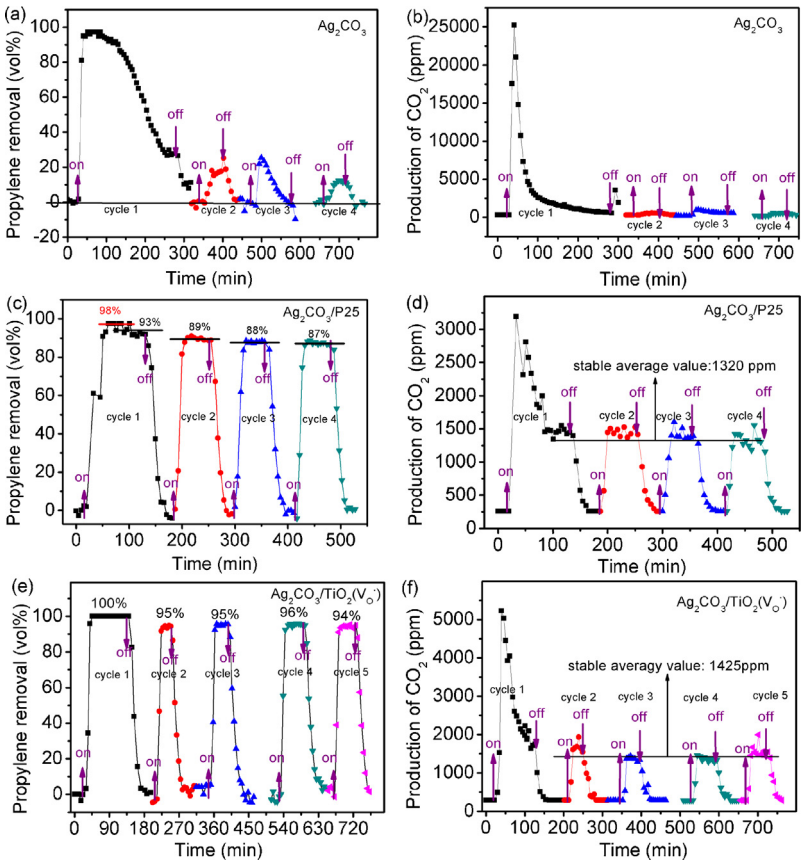

Fig. 6. Visible light photocatalytic activity and stability (a), (c) and (e) in association with production of CO_2 (b), (d) and (f) of samples Ag_2CO_3, Ag_2CO_3/P25 and Ag_2CO_3/TiO_2(V_o•) in system II (a commercial xenon lamp is used as light source, and the quartz reactor is surrounded by a cooling-water channel to eliminate infrared light. A cut filter with λ ≥ 420 nm is inserted between the xenon lamp and the quartz reactor to eliminate UV light. The light intensity of λ = 420 nm irradiated on sample is ca. 40 mW/cm^2).

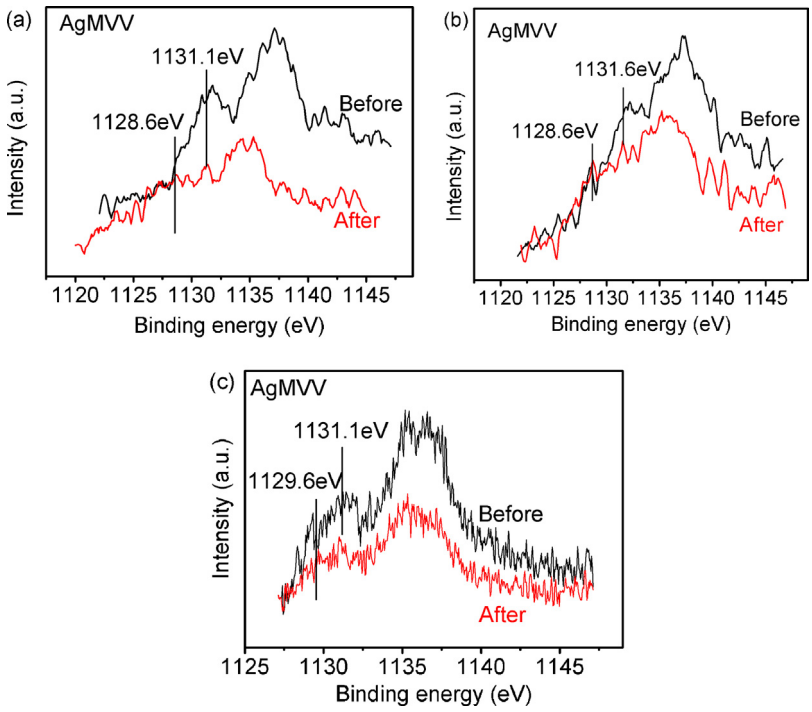

Fig. 7. The comparison of AgMVV XPS spectra of as-prepared Ag_2CO_3 (a), Ag_2CO_3/P25 (b) and $Ag_2CO_3/TiO_2(V_o^{\bullet})$ (c) before irradiation and after 2 h visible light irradiation.

photocatalytic activity of Ag_2CO_3/P25 remains nearly unchanged (average propylene removal rate: 88%). As to $Ag_2CO_3/TiO_2(V_o^{\bullet})$, its photocatalytic activity towards propylene oxidation always retains 100% within 2 h of visible light irradiation in cycle 1, and it is higher than that in reaction system I with a lower light intensity. In the next four cycles, the propylene removal rate over $Ag_2CO_3/TiO_2(V_o^{\bullet})$ remains nearly constant (average value: 95%; Fig. 6e and f). More importantly, over both Ag_2CO_3/P25 and $Ag_2CO_3/TiO_2(V_o^{\bullet})$, no propylene is desorbed from the photocatalyst surface as the xenon lamp is turned off, and the amount of generated CO_2 exactly equals to three times as much as that of photo-degraded propylene (for $Ag_2CO_3/TiO_2(V_o^{\bullet})$: 1425 ppm = 3 × 500 ppm × 95%; for Ag_2CO_3/P25: 1320 ppm = 3 × 500 ppm × 88%). This indicates that, under stronger visible light irradiation (in system II), photo-adsorbed propylene can be completely oxidized into CO_2, and the CO_2 selectivity over both $Ag_2CO_3/TiO_2(V_o^{\bullet})$ and Ag_2CO_3/P25 samples in reaction system II is as much as 100%.

In recent decade, many silver-containing compounds such as $AgGaO_2$, Ag_3VO_4, $AgSbO_3$ and Ag_3PO_4 have been reported to exhibit visible light photocatalytic activity [3–6]. Ag_2CO_3 was also prepared by Dai and exhibits relatively high visible-light photocatalytic activity for the photo-degradation of RhB in aqueous solution [8]. Ag_2CO_3 in the aqueous solution, however, is easily photo-eroded and deactivated owing to photocatalytic decomposition: $Ag_2CO_3 + 2e^- \rightarrow Ag + CO_3^{2-}$. Such a photo-corrosion and deactivation process of Ag_2CO_3 in aqueous solution, fortunately, can be inhibited to some extent by introducing silver nitrate. Thus it can be deduced that the gradual decline of the removal rate of propylene and the concentration of CO_2 over Ag_2CO_3 and Ag_2CO_3/P25 samples should be resulted from the photo-corrosion of Ag_2CO_3, which is further confirmed by XPS, DRS and XRD results of the samples collected after visible light irradiation (Figs. 7 and 8). Namely, the concentration of produced CO_2 over $Ag_2CO_3/TiO_2(V_o^{\bullet})$ is also reduced from the initial level of 4000 ppm to the steady value of 1300 ppm within 50 min of visible light irradiation. This indicates that $Ag_2CO_3/TiO_2(V_o^{\bullet})$ also undergoes decomposition of Ag_2CO_3 under visible light irradiation. To our surprise, the photocatalytic activity of $Ag_2CO_3/TiO_2(V_o^{\bullet})$ does not decline with the increase of irradiation time, which suggests that its visible light photocatalytic mechanism is different from that of Ag_2CO_3/P25.

3.3. XPS, XRD and DRS analyses of various photocatalysts after visible light irradiation

To further confirm the photo-corrosion of various photocatalysts and explore their photocatalytic mechanisms, we conducted XPS, XRD, and UV–vis DRS analyses of Ag_2CO_3, Ag_2CO_3/P25 and $Ag_2CO_3/TiO_2(V_o^{\bullet})$ after visible light irradiation. XPS measurements were comparatively performed to elucidate the changes of chemical state of Ag element after 2 h of visible light irradiation. Because Ag metal and Ag-containing compounds show nearly the same Ag 3d binding energy [19–21], and their Ag Auger MVV peaks often exhibit relatively larger shifts as well as shape changes, we measured the Ag MVV XPS spectra of Ag_2CO_3, Ag_2CO_3/P25 and $Ag_2CO_3/TiO_2(V_o^{\bullet})$ before and after visible light irradiation. As shown in Fig. 7a, the binding energy of Ag_2CO_3 (E_b; AgM4VV) before irradiation is 1131.1 eV. Taking into account the X-ray radiation source (Al $K\alpha$, 1486.6 eV), we can calculate that the kinetic energy (E_k(AgM4VV)) is 355.5 eV (1486.6–1131.1 eV), and it corresponds to Ag^+ of Ag_2CO_3 [19]. After 2 h of visible light irradiation, the E_b peak (AgM4VV) at 1131.1 eV shifts to lower energy of 1128.6 eV and corresponding E_k(AgM4VV) is 358.0 eV (1486.6–1128.6 eV), which indicates that Ag^+ ion in Ag_2CO_3 is reduced to metallic Ag during photocatalytic reaction. Based on the production of CO_2, the photo-corrosion of Ag_2CO_3 in air atmosphere can be described as follow:

$$Ag_2CO_3 + h\nu \rightarrow e^- + h^+ \quad (1)$$

$$Ag_2CO_3 + h\nu \rightarrow Ag_2O + CO_2 \quad (2)$$

$$Ag_2O + 2e^- \rightarrow 2Ag + O^{2-} \quad (3)$$

$$2O^{2-} + 4h^+ \rightarrow O_2 \quad (4)$$

Fig. 7b and c shows the AgM4VV spectra of Ag_2CO_3/P25 and $Ag_2CO_3/TiO_2(V_o^{\bullet})$ in reaction system II before and after irradiation. Similar to what is observed for Ag_2CO_3, the AgM4VV peaks

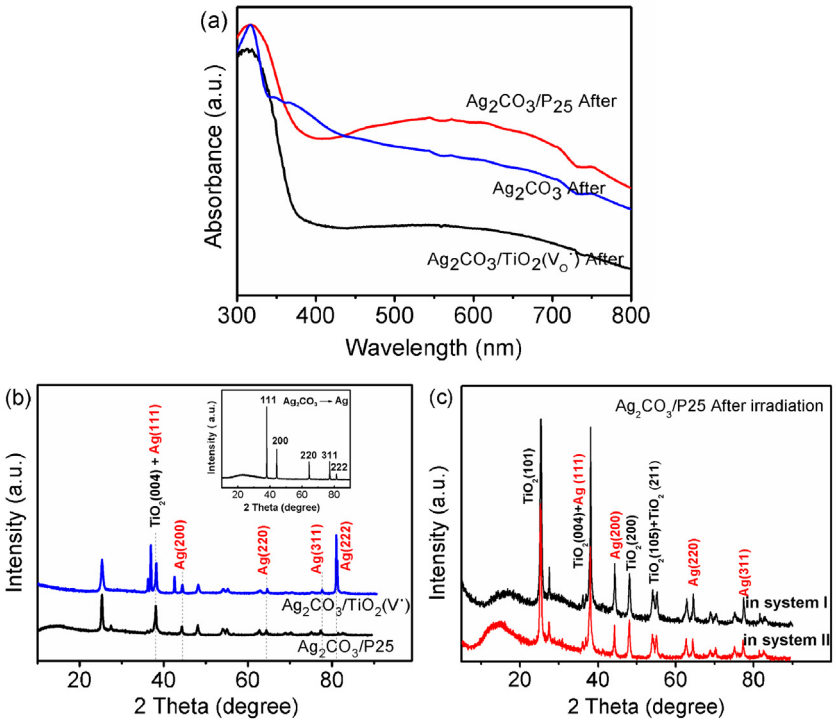

Fig. 8. UV–vis absorption spectra of samples Ag_2CO_3, $Ag_2CO_3/TiO_2(V_o^{\bullet})$ and Ag_2CO_3/P25 after visible light irradiation for 2 h (a); XRD patterns of $Ag_2CO_3/TiO_2(V_o^{\bullet})$ and Ag_2CO_3/P25 after visible light irradiation for 2 h (b), the inset displays XRD pattern of Ag_2CO_3 after visible light irradiation for 2 h; comparison of XRD patterns of Ag_2CO_3/P25 after 2 h visible light irradiation in two reaction systems (c).

of Ag_2CO_3/P25 and $Ag_2CO_3/TiO_2(V_o^{\bullet})$ also shift towards lower binding energy, which implies that Ag^+ ions in Ag_2CO_3/P25 and $Ag_2CO_3/TiO_2(V_o^{\bullet})$ are photo-corroded into Ag metal particles. This is in consistent with DRS and XRD results of the two samples after irradiation (Fig. 8a and b).

UV–vis DRS and XRD analyses were conducted after 2 h visible light irradiation of system II to determine the transformation of various photocatalysts during the photo-degradation process of propylene. The UV–vis diffuse reflectance spectra of photocatalysts Ag_2CO_3, Ag_2CO_3/P25 and $Ag_2CO_3/TiO_2(V_o^{\bullet})$ after 2 h visible light irradiation in system II are shown in Fig. 8a. It can be seen that, after 2 h of visible light irradiation, both Ag_2CO_3/P25 and $Ag_2CO_3/TiO_2(V_o^{\bullet})$ show a similar broad absorption in the range of 400–800 nm, which is due to the surface plasmon resonance (SPR) of Ag^0 particles [22,23]. This further confirms that Ag_2CO_3/P25 and $Ag_2CO_3/TiO_2(V_o^{\bullet})$ are indeed photo-corroded, since SPR is a collective oscillation of electrons in metallic nanoparticles which are excited by incident light. In the meantime, the optical properties associated with surface plasmon resonance are highly dependent on nanoparticles' size, shape and local dielectric environment [24–26]. As for Ag_2CO_3, the broad absorption band in the visible light region is different from that of Ag_2CO_3/P25 and $Ag_2CO_3/TiO_2(V_o^{\bullet})$, which may be due to the large micro-size of Ag_2CO_3 particle. Fig. 8b displays the XRD patterns of Ag_2CO_3, Ag_2CO_3/P25 and $Ag_2CO_3/TiO_2(V_o^{\bullet})$ after 2 h irradiation of system II. It can be seen that Ag_2CO_3 tested in system II for 2 h shows five intense diffraction peaks at 38.2°, 44.2°, 64.4°, 77.4°, and 80.7°, and these XRD peaks correspond to the (1 1 1), (2 0 0), (2 2 0), (3 1 1), and (2 2 2) lattice planes of cubic structure of Ag (see the inset in Fig. 8b). This, in combination with the absence of any diffraction peak of monoclinic Ag_2CO_3, also confirms that 2 h visible light irradiation in system II causes photo-corrosion of Ag_2CO_3 thereby yielding metallic Ag. Similar photo-corrosion of Ag_2CO_3/P25 is also observed after 2 h irradiation in system II, which well explains why Ag_2CO_3/P25 exhibits highly efficient photo-oxidation activity towards propylene in system II. Comparing the XRD patterns of Ag_2CO_3/P25 after irradiation in system I and II (Fig. 8c), we can see that they show no significant differences. This implies that photocatalyst Ag_2CO_3/P25 tested in system I and system II undergoes the same structure transformation to afford metallic Ag *via* photo-corrosion. Thus we can further infer that the higher intensity of light irradiated on to-be-tested samples in system II contributes to the highly efficient photo-oxidation activity of Ag_2CO_3/P25 towards propylene therein. Moreover, $Ag_2CO_3/TiO_2(V_o^{\bullet})$ tested in system II shows much strong (2 2 2) diffraction peak of cubic Ag, which is possibly correlated with the nano-rod morphology of $TiO_2(V_o^{\bullet})$. In other words, Ag nanoparticles reduced from Ag_2CO_3 tend to dwell on the surface of $TiO_2(V_o^{\bullet})$ matrix and grow along the nano-rods. As a result, the enhanced photo-corrosion of Ag_2CO_3 along $TiO_2(V_o^{\bullet})$ nano-rods gives rise to more Ag nanoparticles thereby causing stronger (2 2 2) diffraction. In addition, $Ag_2CO_3/TiO_2(V_o^{\bullet})$ tested in system II shows two unknown diffraction peaks at 36.2° and 42.7°, and they are worth further investigation in future.

3.4. *Visible light photocatalytic mechanism of Ag_2CO_3/P25 and $Ag_2CO_3/TiO_2(V_o^{\bullet})$ in systems I and II*

Based on the abovementioned XPS, DRS and XRD results of Ag_2CO_3/P25 and $Ag_2CO_3/TiO_2(V_o^{\bullet})$ samples after illumination, it can be concluded that Ag_2CO_3 deposited on the surface of TiO_2 matrix (P25 TiO_2 or $TiO_2(V_o^{\bullet})$) is photo-corroded during photocatalytic process to yield metallic Ag thereby resulting in Ag/P25 (or $Ag/TiO_2(V_o^{\bullet})$) from Ag_2CO_3/P25 (or $Ag_2CO_3/TiO_2(V_o^{\bullet})$). In other words, the photocatalytic activity of Ag_2CO_3/P25 and $Ag_2CO_3/TiO_2(V_o^{\bullet})$ towards propylene degradation is gradually transformed to that of Ag/P25 and $Ag/TiO_2(V_o^{\bullet})$ towards propylene degradation under visible light irradiation. In reaction system I with a weak light intensity (9 mW/cm^2), Ag/P25 exhibits nearly no visible light activity for the degradation of propylene, although it exhibits apparent photo-induced adsorption and desorption ability

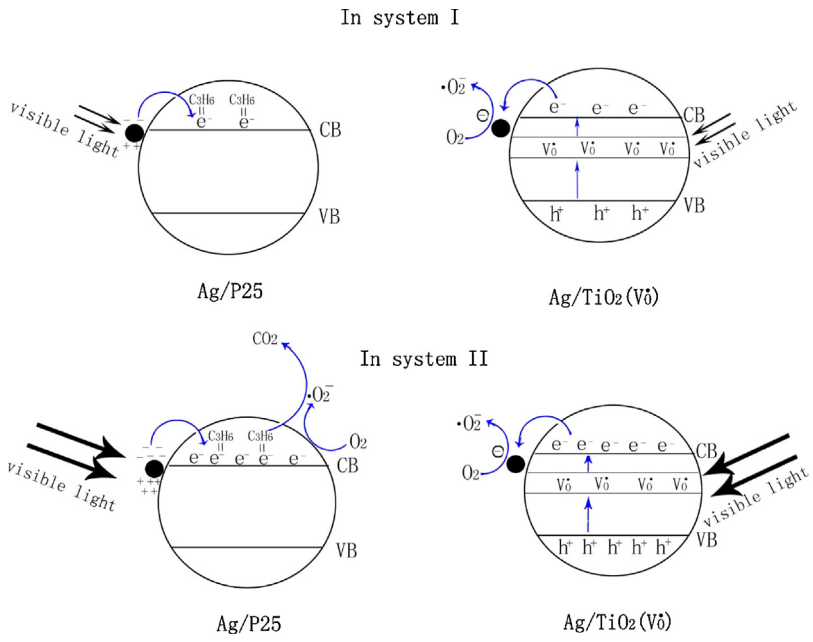

Scheme 1. Action mechanisms of Ag/P25 and Ag/TiO_2(V_o•) generated from Ag_2CO_3/P25 and Ag_2CO_3/TiO_2(V_o•) towards visible light photodegradation of propylene in system I and system II.

for propylene. The reason lies in that the surface plasmon resonance of Ag^0 particles in Ag/P25 causes an apparent plasmon absorption band in the wavelength range of 450–700 nm; but P25-TiO_2 cannot be excited by visible light, due to too large band gap. Upon weak visible light excitation in system I, a few electrons in the filled d-band are excited to electronic states above the Fermi level in the *sp* conduction band of silver nanoparticles that are attached to P25-TiO_2 matrix. Although many researches have demonstrated that electron transfer from the conduction band of the semiconductor to the noble metal such as Au and Ag can improve the efficiency of photocatalytic redox processes, The electron injection from Au or Ag nanoparticle to TiO_2 on SPR excitation has been proven truly happened in Au/TiO_2 and Ag/TiO_2 systems and the number of electrons injected into TiO_2 is proportional to the excitation light intensity [27–30]. Therefore, under weak visible light excitation in system I, only a few electrons can be excited to overcome a 0.4 eV Schottky barrier on Ag/TiO_2, and fewer electrons are transferred to the photocatalyst surface and trapped by adsorbed O_2 generating $^{\bullet}O_2^-$. As a result, only few photo-adsorbed propylene are oxidized into CO_2 in system I, while most of adsorbed propylene is desorbed from the surface of P25-TiO_2 upon light turning off. Under intense visible light irradiation in system II, however, numerous electrons are excited to overcome the Schottky barrier and transferred to the photocatalyst surface thereby yielding sufficient $^{\bullet}O_2^-$ and resulting in a high degradation rate of propylene.

Differing from Ag/P25, Ag/TiO_2(V_o•) displays a high propylene removal rate of 90% and a perfect CO_2 selectivity of 100% in system I. This implies that Ag/P25 and Ag/TiO_2(V_o•) may undergo different photocatalytic mechanisms under visible light irradiation, as illustrated in Scheme 1. Namely, a sub-band resulted from SETOV is generated in the TiO_2(V_o•) matrix of Ag/TiO_2(V_o•); under weak (system I) or intense (system II) visible light excitation, the electrons trapped on oxygen vacancies (i.e., SETOV) can be excited to the conduction band of TiO_2(V_o•) and captured by silver particles on the surface of TiO_2(V_o•). A Schottky junction is formed between Ag and TiO_2 right upon their contact, because TiO_2 has a higher Fermi level than Ag [31–33]. Resultant Schottky barrier hinders electrons to cross the boundary and transfer from Ag to TiO_2, thereby suppressing the electron–hole recombination in photocatalytic process. It is generally accepted that metallic Ag nanoparticle functions as an electron sink to accept photogenerated electrons from excited semiconductor thereby facilitating the formation of superoxide anion radical ($^{\bullet}O_2^-$) which is capable of degrading organic compound like propylene. Therefore, Ag/TiO_2(V_o•) (or Ag_2CO_3/TiO_2(V_o•)) exhibits very high visible light photocatalytic activity towards propylene degradation in both reaction systems.

4. Conclusions

P25-TiO_2 and TiO_2(V_o•) were separately used as the precursors to prepare two kinds of Ag_2CO_3/TiO_2 composite photocatalysts, Ag_2CO_3/P25 and Ag_2CO_3/TiO_2(V_o•), by precipitation method, and the photocatalytic activity of two as-prepared photocatalysts was evaluated in relation to the photo-corrosion of Ag_2CO_3. It has been found that Ag_2CO_3 on the surface of P25-TiO_2 or TiO_2(V_o•) undergoes photo-corrosion generating metallic Ag nanoparticles under visible light irradiation. As a result, the synergistic effect between the sub-band excitation of TiO_2 by SETOV and the electron capture of silver nanoparticles accounts for the highly efficient and stable photocatalytic activity of Ag_2CO_3/TiO_2(V_o•) (or its photo-corroded product Ag/TiO_2(V_o•)) towards propylene degradation under visible light irradiation in both system I and system II. Besides, Ag/P25 exhibits nearly no visible light activity for the degradation of propylene in reaction system I, although it exhibits apparent photo-induced adsorption and desorption ability for propylene. This is because the surface plasmon resonance of Ag^0 particles in Ag/P25 causes an apparent plasmon absorption band in the wavelength range of 450–700 nm, but P25-TiO_2 with a too large band gap cannot be excited by visible light. However, under intense visible light irradiation in system II, numerous electrons are excited to overcome the Schottky barrier and transferred to photocatalyst surface, thereby affording sufficient $^{\bullet}O_2^-$ and providing a high degradation rate of propylene. In one word, elevating visible light intensity favors to increase the photocatalytic activity of Ag_2CO_3/P25 and Ag_2CO_3/TiO_2(V_o•) photocatalysts towards propylene degradation under visible light irradiation, and the two kinds of photocatalysts undergo different action mechanisms towards visible light catalytic degradation of propylene.

Acknowledgment

The authors acknowledge the financial support provided by the Science & Technology Research Project of Henan province (Grant no. 14B150038 and 142300410117), and they also would like to thank Professor Laigui Yu for critically reviewing the manuscript.

Appendix A. Supplementary data

Supplementary data associated with this article can be found, in the online version, at http://dx.doi.org/10.1016/j.apcatb.2014.04.020.

References

[1] H. Kato, H. Kobayashi, A. Kudo, J. Phys. Chem. B 106 (2002) 12441–12447.
[2] R. Konta, H. Kato, H. Kobayashi, A. Kudo, Phys. Chem. Chem. Phys. 5 (2003) 3061–3065.
[3] X.X. Hu, C. Hu, J.H. Qu, Mater. Res. Bull. 43 (2008) 2986–2997.
[4] T. Kako, N. Kikugawa, J.H. Ye, Catal. Today 131 (2008) 197–202.
[5] Y. Maruyama, H. Irie, K. Hashimoto, J. Phys. Chem. B 110 (2006) 23274–23278.
[6] Z.G. Yi, J.H. Ye, N. Kikugawa, T. Kako, S.X. Ouyang, H.S. Williams, H. Yang, J.Y. Cao, W.J. Luo, Z.S. Li, Y. Liu, R.L. Withers, Nat. Mater. 9 (2010) 559–564.
[7] C.W. Xu, Y.Y. Liu, B.B. Huang, H. Li, X.Y. Qin, X.Y. Zhang, Y. Dai, Appl. Surf. Sci. 257 (2011) 8732–8736.
[8] G.P. Dai, J.G. Yu, G. Liu, J. Phys. Chem. C 116 (2012) 15519–15524.
[9] H.J. Dong, G. Chen, J.X. Sun, C.M. Li, Y.G. Yu, D.H. Chen, Appl. Catal., B: Environ. 134–135 (2013) 46–54.
[10] Y. Wang, P.H. Ren, C.X. Feng, X. Zheng, Z.G. Wang, D.L. Li, Mater. Lett. 115 (2014) 85–88.
[11] J.J. Yang, Z.S. Jin, X.D. Wang, W. Li, J.W. Zhang, S.L. Zhang, X.Y. Guo, Z.J. Zhang, Dalton Trans. 20 (2003) 3898–3901.
[12] M. Zhang, Z.S. Jin, J.W. Zhang, X.Y. Guo, J.J. Yang, W. Li, X.D. Wang, Z.J. Zhang, J. Mol. Catal., A: Chem. 217 (2004) 203–210.
[13] S.L. Zhang, W. Li, Z.S. Jin, J.J. Yang, J.W. Zhang, Z.L. Du, Z.J. Zhang, J. Solid State Chem. 177 (2004) 1365–1371.
[14] L. Qian, Z.S. Jin, J.W. Zhang, Y.B. Huang, Z.J. Zhang, Z.L. Du, Appl. Phys. A: Mater. Sci. Process. 80 (2005) 1801–1805.
[15] Y. Wang, C.X. Feng, M. Zhang, J.J. Yang, Z.J. Zhang, Appl. Catal., B: Environ. 100 (2010) 84–90.
[16] Y. Wang, C.X. Feng, M. Zhang, J.J. Yang, Z.J. Zhang, Appl. Catal., B: Environ. 104 (2011) 268–274.
[17] Y. Wang, M.J. Jing, M. Zhang, J.J. Yang, Catal. Commun. 20 (2012) 46–50.
[18] C.X. Feng, J.W. Zhang, R. Lang, Z.S. Jin, Z.S. Wu, Z.J. Zhang, Appl. Surf. Sci. 257 (2011) 1864–1870.
[19] X.D. Wang, Z.S. Jin, C.X. Feng, Z.J. Zhang, H.X. Dang, J. Solid State Chem. 178 (2005) 638–644.
[20] J.F. Moulder, W.F. Stickle, P.E. Sobol, K.D. Bomben, Handbook of X-Ray Photoelectron Spectroscopy, Perkin-Elmer Corporation, Eden Prairie, MN, 1992.
[21] G.B. Hoflund, Z.F. Hazos, Phys. Rev. B: Condens. Matter 62 (2000) 11126–11133.
[22] J.H. He, I. Ichinose, T. Kunitake, A. Nakao, Langmuir 18 (2002) 10005–10010.
[23] H. Zhang, G. Wang, D. Chen, X.J. Lv, J.H. Li, Chem. Mater. 20 (2008) 6543–6549.
[24] J. Jiang, H. Li, L.Z. Zhang, Chem. Eur. J. 18 (2012) 6360–6369.
[25] H. Wang, D.W. Brandl, P. Nordlander, N.J. Halas, Acc. Chem. Res. 40 (2006) 53–62.
[26] Z.C. Wang, J.H. Liu, W. Chen, Dalton Trans. 41 (2012) 4866–4870.
[27] L.C. Du, A. Furube, K. Hara, R. Katoh, M. Tachiya, Thin Solid Films 518 (2009) 861–864.
[28] L.C. Du, A. Furube, K. Yamamoto, K. Hara, R. Katoh, M. Tachiya, J. Phys. Chem. C 113 (2009) 6454–6462.
[29] L.C. Du, A. Furube, K. Hara, R. Katoh, M. Tachiya, J. Photochem. Photobiol., C 15 (2013) 21–30.
[30] L.S. Daniel, H. Nagai, M. Sato, J. Mater. Sci. 48 (2013) 7162–7170.
[31] H.W. Chen, Y. Ku, Y.L. Kuo, Chem. Eng. Technol. 30 (2007) 1242–1247.
[32] Y.Y. Wen, H.M. Ding, Y.K. Shan, Nanoscale 3 (2011) 4411–4417.
[33] S.S. Mandal, A.J. Bhattacharyya, J. Chem. Sci. 124 (2012) 969–978.